10.5-T MRI Volume Excitation Using Traveling-Wave Microstrip Probes

Patrick Bluem and Zoya Popovic
Electrical, Computer, and Energy Engineering
University of Colorado Boulder
Boulder, Colorado 80303
Email: zoya.popovic@colorado.edu

***Abstract*—This paper presents a volume excitation study of a human-sized MRI bore at 10.5 T using a circular patch, an interdigitated capacitor probe (ICP) array, and a combination of the two. Compared to an experimentally verified single patch probe excitation, the ICP array allows for B_1^+ shimming by modifying the magnitude and phase of the elements to fill the field void left near the edges of an uniform phantom. Simulations using full-wave FDTD show an increase in field coverage inside of the uniform phantom which can further be improved by the addition of a simple, passive slow-wave helical boundary structure.**

***Index Terms*—FDTD, Interdigitated Capacitors, Patch Probe, Ultra-High Field MRI**

I. Introduction

High-field wide-bore MRI (>4 T) is used to increase the spatial resolution of MRI medical images, especially for localized cases, e.g., in the head [1] or leg [2]. A human-sized bore at the corresponding Larmor frequencies (447 MHz at 10.5 T) becomes an over-moded waveguide when loaded with a dielectric body. That implies traveling waves inside the bore which can constructively and destructively interfere with the MR excitation creating undesired peaks and nulls. In this paper we examine excitation methods that improve field distribution inside of a uniform cylindrical phantom (ε_r=81 and σ=0.4 S/m). Fig. 1a shows the general setup with dimensions corresponding to the magnet at the Center for Magnetic Resonance Research (University of Minnesota). Instead of the usual coils, printed radiators are increasingly implemented in ultra-high field systems. In [3], a radial array of 8 stripline radiating elements is used to excite the head for a 7 T system. Other methods extend this to first and second harmonic microstrip radiators [4], segmented loaded dipoles [5], and tailored microstrip radiators for an even current distribution [6].

Fig. 1a shows the setup for the single circular patch probe excitation where the distance d between the probe and the phantom can be varied. Fig. 1 also shows three excitations discussed in this paper. For validation purposes, two different numerical solvers are used, Ansys HFSS (FEM) and Zurich Med Tech Sim4Life (FDTD). All simulations show the sagittal cut of the phantom.

II. Probe Designs

A single patch probe (Fig. 1b), similar to the one in [7], is excited to observe the simplest case results at 10.5 T so they can be compared to simulations. The probe is placed 15 cm from the phantom, as this was found to balance the near-field and the propagated components of the MR excitation. The field pattern obtained in the experimental MR image in Fig. 2a has strong similarity with the simulated $|B_1^+|$ field shown in Fig.

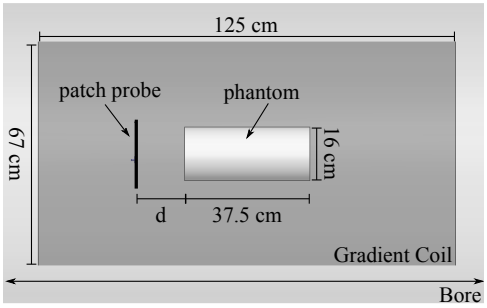

(a)

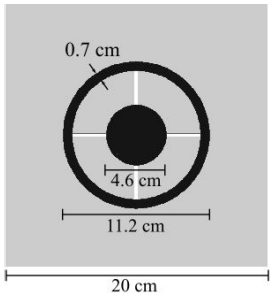

(b)

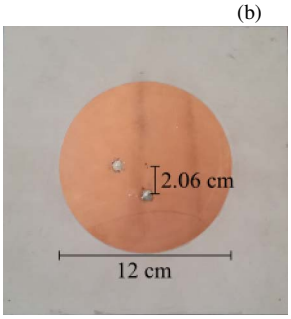

(c)

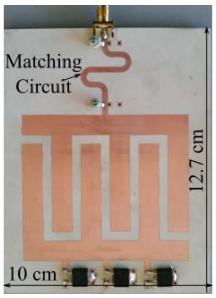

(d)

Fig. 1. (a) Sagittal view of the dimensions under the gradient coil for the 10.5 T Siemens system. The dark gray region is the region internal to the gradient coil. 10.5 T (b, c) circular patch probe and (d) interdigitated capacitor traveling-wave probe.

978-1-5090-6360-4/17/$31.00 ©2017 IEEE

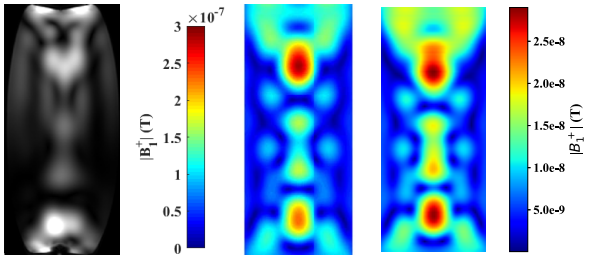

(a) (b) (c)

Fig. 2. Single probe experiment results for: (a) MR image taken using a gradient recalled echo sequence for a FOV of 16.25x40 cm^2 with a small flip angle (b) Simulated FEM patch probe (Fig. 1b) excitation. Simulation is normalized to 1 W excitation. (c) Simulated FDTD patch probe (Fig. 1c) excitation normalized to 1 V.

2b. Due to the electrically large size of the phantom ($\approx 2\lambda$), the excited field modes are much more complex compared to results found in lower field system, [2], and creating a uniform field excitation throughout the phantom becomes difficult. One of the goals of this paper is to demonstrate a few methods to improve the field distribution and uniformity in the upper region of the phantom where the head would be located in a human-sized bore.

To improve on the single patch setup, two different types of probes are studied for the system shown in Fig. 1. The first is the typical quadrature fed circular patch probe as used in [2] which creates a right handed circular polarized excitation by phasing the feeds 90° apart. This probe has been used extensively in traveling wave MRI applications as it is simple and can be placed such that it is not loaded by the imaging volume, requiring no tuning between different phantoms or patients. The probe can be seen in Fig. 1c with dimensions for Rogers 3010 substrate ($\varepsilon_r = 11.1$) of 1.27 mm thickness. The two coaxial feeds are 2.06 cm from the center of the probe and both exhibit a return loss better than 10 dB at 447 MHz in free-space.

The second probe is a traveling-wave interdigitated capacitor probe [8] and shown in Fig. 1d on Rogers 6010 (ε_r=10.6) 1.27 mm substrate. The fingers are 4.66 cm long, 0.95 cm wide, and spaced 4.4 mm apart. Three 75 Ω, 25 W resistors are added in parallel to balance the current across the fingers of the probe. Simulations show that a 25 Ω load allows 32 % of the power to be dissipated in the load which forces current across the lower fingers. Three loads are used in parallel to reduce the power consumption by each resistor. The probe exhibits an unloaded free-space return loss of 9.5 dB at 447 MHz.

Due to the high anisotropy and variation between substrate panels, a Π network consisting of shunt capacitors and series length of line is added for tuning. The probes are placed in a 12-element cylindrical array and close to the imaging volume. Therefore, some coupling that can result in a need for tuning is expected. With a separation of 3 cm between the probes and the phantom, the match stays close to the expected free-space value. The goal behind a probe array is to create a volume excitation and improve the spatial resolution of the received MR signal. To control polarization, a phase offset can be applied at the probe feeds, and in this work a 60° incremental phase offset is used as a starting point for optimization.

Each probe is simulated individually using full-wave FDTD. The resulting fields are post-processed using Python by adding a relative phase and using superposition to model the entire array. The optimization technique employed is sequential least squares to minimize the standard deviation of B_1^+ inside the phantom. The optimization parameters are the excitation phases and amplitudes. The trivial solution of the problem will be removing the contribution of the ICPs such that the magnitude of each ICP's field is only allowed to reduce to 1/4 of the single circular probe field. This is found to be the best balance between the ICP array excitation and the single circular probe excitation. In section IV of this paper, the phase refers to the relative incremental phase in the array for both the first and second row of ICP array. The circular patch probe is at 0 phase and 1 V excitation on each feed.

III. Performance of Interdigitated Capacitor Probe Volume Excitation

The setup of the ICP array in Fig. 3 encircles the phantom in two rows. The row closest to the phantom will be referred to as the first row. With proper phasing, the ICP array can have a near symmetrical field excitation compared to 60 degree incremental phasing as shown in Fig. 4. Compared to the single circular probe measurements in Fig. 2, the ICP array fills the field void left on the edges of the phantom. To ensure the ICP array elements do not couple, the simulation is repeated in HFSS and shows -30 dB coupling between probes. This can be confirmed in Sim4Life where the electric field near the copper of the adjacent probe is 20 dB down from the field excited in the probe, and 60 dB down from the field 1 cm off the probe.

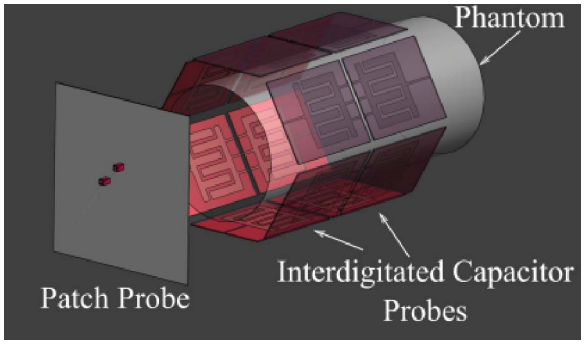

Fig. 3. Sim4Life setup with the ICP array encircling the phantom.

The ICP array can also be combined with the circular patch probe (Fig. 1c) to improve the field distribution as shown in Fig. 5. Compared to the solution of Fig. 2, there is significantly more coverage of the field inside the phantom. However, there are still large peaks with relatively close nulls, which would result in a poor medical image. The field peaks can be minimized by increasing the magnitude of the ICP excitations, but the coronal cut becomes nearly zero along the phantom axis. This shows that the scaling of the ICP array has a large influence on the entire field distribution due to

978-1-5090-6360-4/17/$31.00 ©2017 IEEE

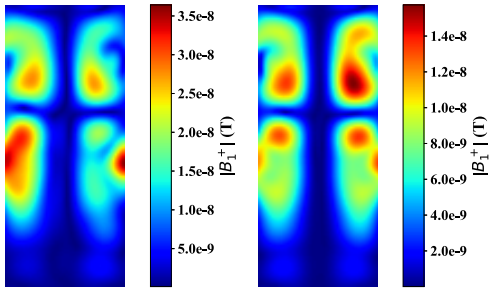

(a) (b)

Fig. 4. Phased ICP array (a) with 60 degree incremental phase and magnitude 1/2 of the circular probe and (b) with phasing [23.88, 62.04, 41.86, 37.76, 36.66, 54.03] for the first row and [15.04, 54.78, 37.3, 35.63, 42.72, 50.25] for the second row and magnitude 1/4 of the circular probe.

the constructive and destructive interference of the fields from each probe. Validation of the designed setup is performed using Ansys HFSS with the complete setup of 12 ICPs and circular patch probe. For the same setup and phasing as in Fig. 5b, Fig. 6b shows similarity in the excited mode structure. Unfortunately, the HFSS simulation runs out of computational resources resulting in a coarser mesh and affecting the field solution.

In order to improve the sharp gradient of the field, a counter-clockwise rotating quadrifilar helix placed 2 cm off of the phantom as shown in Fig. 8 is added to the setup. In [9], a

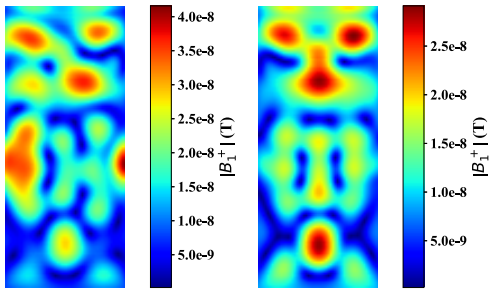

(a) (b)

Fig. 5. Circular probe and phased ICP array (a) with 60 degree incremental phase and magnitude 1/2 of the circular probe and (b) with phasing [18.69, 70.39, 43.62, 32.18, 31.9, 59.69] for the first row and [1.0, 35.79, 34.01, 35.24, 33.93, 38.09] for the second row and magnitude 1/4 of the circular probe.

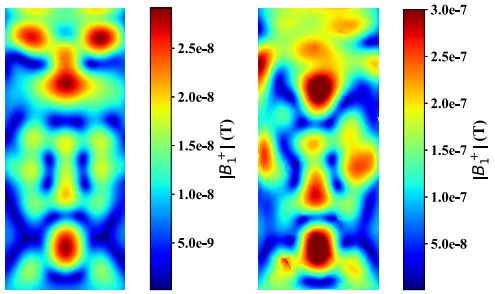

(a) (b)

Fig. 6. Circular probe and phased ICP array simulated using (a) Sim4Life (FDTD) and (b) HFSS (FEM).

quadrifilar helix fed by four generators in quadrature is shown to have a very similar field distribution to a single circular patch excitation at 7 T. In contrast, here the helix is not fed but rather serves as a boundary structure that changes the modal content without significantly reducing the overall magnitude of the field while reducing the gradients.

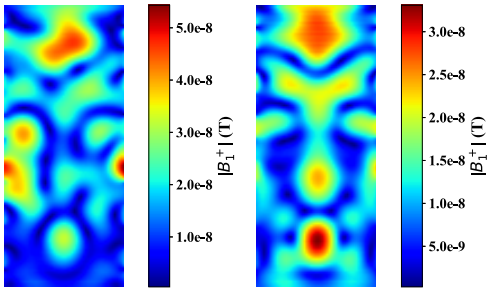

(a) (b)

Fig. 7. Circular probe and phased ICP array with counter-clockwise helix around the phantom. (a) 60 degree incremental phase and magnitude 1/2 of the circular probe. (b) phasing [100.29, 40.51, 25.69, 42.88, 59.72, 30.05] for the first row and [123.66, 94.15, 24.65, 31.63, 20.04, 93.87] for the second row and magnitude 1/4 of the circular probe.

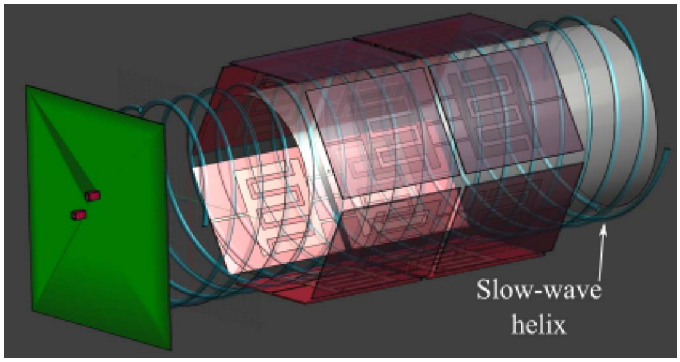

Fig. 8. Sim4Life setup showing the counter-clockwise rotating helix encircling the phantom.

IV. Conclusion

The presented study of volume excitations of a wide-bore MRI at 10.5 T shows that an array of interdigitated capacitor probes with amplitude and phase variation can improve the field distribution inside of a uniform water phantom. Compared to an experimentally verified single patch probe excitation, the ICP array allows for B_1^+ shimming by modifying the magnitude and phase of the elements to fill the void left near the edges of an uniform phantom. Experimental results for the single patch probe excitation is verified using both FEM and FDTD numerical methods. Additionally, simulations using an FDTD solver show an increase in field coverage inside of the uniform phantom which can further be improved by the addition of a simple, passive slow-wave helical boundary structure.

978-1-5090-6360-4/17/$31.00 ©2017 IEEE

V. Acknowledgments

The authors acknowledge support by the National Science Foundation under a collaborative research grant ECCS 1307614 at the University of Colorado, Boulder. We are also grateful to Dr. Pierre-Francois Van de Moortele and Dr. Gregor Adriany at CMRR, University of Minnesota, and Dr. Andrew Kiruluta at Harvard University.

References

[1] M. A. Ertrk, X. Wu, Y. Eryaman, P.-F. Van de Moortele, E. J. Auerbach, R. L. Lagore, L. DelaBarre, J. T. Vaughan, K. Ugurbil, G. Adriany, and G. J. Metzger, "Toward imaging the body at 10.5 tesla," *Magnetic Resonance in Medicine*, 2016.

[2] D. Brunner, D. Z. Nicola, F. Jurg, P. Jan, and P. K. P., "Travelling-wave nuclear magnetic resonance," *Nature*, vol. 457, no. 7232, pp. 994–998, Feb. 2009.

[3] G. Adriany, P.-F. Van de Moortele, F. Wiesinger, S. Moeller, J. P. Strupp, P. Andersen, C. Snyder, X. Zhang, W. Chen, K. P. Pruessmann, P. Boesiger, T. Vaughan, and K. Ugurbil, "Transmit and receive transmission line arrays for 7 tesla parallel imaging," *Magnetic Resonance in Medicine*, vol. 53, no. 2, pp. 434–445, 2005. [Online]. Available: http://dx.doi.org/10.1002/mrm.20321

[4] B. Wu, C. Wang, J. Lu, Y. Pang, S. J. Nelson, D. B. Vigneron, and X. Zhang, "Multi-channel microstrip transceiver arrays using harmonics for high field MR imaging in humans," *IEEE Transactions on Medical Imaging*, vol. 31, no. 2, pp. 183–191, Feb 2012.

[5] A. J. Raaijmakers, M. Italiaander, I. J. Voogt, P. R. Luijten, J. M. Hoogduin, D. W. Klomp, and C. A. van den Berg, "The fractionated dipole antenna: A new antenna for body imaging at 7 tesla," *Magnetic Resonance in Medicine*, vol. 75, no. 3, pp. 1366–1374, 2016.

[6] S. M. Sohn, L. DelaBarre, A. Gopinath, and J. T. Vaughan, "RF head coil design with improved RF magnetic near-fields uniformity for magnetic resonance imaging (MRI) systems," *IEEE Transactions on Microwave Theory and Techniques*, vol. 62, no. 8, pp. 1784–1789, Aug 2014.

[7] P. Bluem, A. Tonyushkin, D. Deelchand, G. Adriany, P. F. V. de Moortele, A. J. M. Kiruluta, and Z. Popovic, "Travelling-wave excitation for 16.4T small-bore MRI," in *Microwave Symposium (IMS), 2015 IEEE MTT-S International*, May 2015, pp. 1–4.

[8] A. Munir and E. K. Sari, "Printed traveling wave antenna composed of interdigital capacitor structure for wireless communication application," in *2015 International Seminar on Intelligent Technology and Its Applications (ISITIA)*, May 2015, pp. 441–444.

[9] M. Ilic, A. Tonyushkin, N. Sekeljic, P. Athalye, and B. M. Notaros, "RF excitation in 7 tesla MRI systems using monofilar axial-mode helical antenna," in *Antennas and Propagation USNC/URSI National Radio Science Meeting, 2015 IEEE International Symposium on*, July 2015, pp. 1346–1347.

978-1-5090-6360-4/17/$31.00 ©2017 IEEE